Colloids and Surfaces B: Biointerfaces 202 (2021) 111641

Contents lists available at ScienceDirect

Colloids and Surfaces B: Biointerfaces

journal homepage: www.elsevier.com/locate/colsurfb

# Self-assembly and thermoreversible rheology of perfluorocarbon nanoemulsion-based gels with amphiphilic copolymers

Jiachun Shen [a,1], Xiaoming Pan [b,1], Surita R. Bhatia [a,*]

[a] Department of Chemistry, Stony Brook University, Stony Brook, NY 11794-3400, USA
[b] Department of Chemical Engineering, University of Massachusetts Amherst, Amherst, MA 01003, USA

ARTICLE INFO

*Keywords:*
Oxygen
Blood substitute
Gel
Perfluorocarbon
Emulsion
Rheology

ABSTRACT

Perfluorocarbon (PFC) nanoemulsions have great potential in biomedical applications due to their unique chemical stability, biocompatibility, and possibilities for enhanced oxygen supply. The addition of amphiphilic block copolymers promotes the formation and long-term stability of emulsion-based gels. In this work, we report the systematic study of the impact of adding amphiphilic triblock copolymers to water-in-perfluorocarbon nanoemulsions on their structure and viscoelasticity, utilizing small-angle neutron and X-ray scattering (SANS and SAXS) and rheology. We find that an intermediate concentration of copolymer yields the highest strength of attraction between droplets, corresponding to a maximum in the elasticity and storage modulus. The stability and viscoelastic moduli can be tuned via the amount of copolymer and surfactant along with the volume fraction of aqueous phase. SANS provides the detail on nanostructure and can be fit to a spherical core-shell form factor with a square-well hard sphere structure factor. The PFC nanoemulsion system displays thermoresponsive and thermoreversible properties in temperature sweeps.

## 1. Introduction

Soft materials such as emulsions, polymer micelles and liposomes, have been extensively applied in a variety of practical applications including drug delivery [1,2], material synthesis [3,4], and separation [5] due to their superior ability to transport and transfer loadings. However, application of emulsions in biomedical fields has not been fully realized, due to the limited stability of emulsion droplets [6,7] and the potential leakage of cargo from the core of emulsion [8,9]. Perfluorocarbon (PFC) materials have great potential for biomedical applications due to the outstanding chemical stability and biological inertness arising from the replacement of hydrogen atoms by fluorine [10]. These strong covalent C–F bonds yield relatively low van der Waals forces between fluorocarbon chains and low cohesive energy in liquid state, leading to valuable properties including high fluidity, high gas solubility, high vapor pressure and low surface tension [11,12]. Perfluorooctyl bromide (PFOB) is one of several well-explored PFC materials that is approved for medical use by FDA and is used as a contrast material for CT, MRI and ultrasound imaging, especially for hepatosplenography and tumor-imaging [13–15]. In addition, perfluorocarbon-based materials have great potential in the application of enhancing oxygen transport, where they have been demonstrated to show 20-fold higher capacity to dissolve oxygen than aqueous solutions. In our previous work, PFOB-containing alginate gels exhibited the promotion of oxygen availability and oxygen uptake rates, which led to the enhancement in metabolic activity and functionality of HepG2 cells, while common aqueous hydrogels could hardly achieve this without the addition of PFCs or other oxygen-carrying species [16,17]. Due to the mentioned outstanding properties, the related PFC-in-water and water-in-PFC emulsions have already been explored in many biomedical fields such as liquid-assisted ventilation [18,19], blood substitutes [17,20] and microfluidic devices [21]. The reverse of a traditional oil-in-water emulsion system, a water-in-PFC emulsion is composed of liquid PFC as the continuous oil phase with water droplets and fully or partially fluorinated surfactant to stabilize the emulsions [22,23]. By gelling such a PFC-based emulsion system, a stable and robust emulsion gel material with good biocompatibility could be achieved for more potential uses in biomedical applications. The structure and rheology of PFC-based systems can significantly impact the use in potential applications. For example, in PFC emulsions, the size of PFC droplets influences the oxygen transport process [24,25], and for cell encapsulation applications, it is important that the system behaves as a mechanically

* Corresponding author.
*E-mail address:* surita.bhatia@stonybrook.edu (S.R. Bhatia).
[1] Both authors contributed equally to this manuscript.

https://doi.org/10.1016/j.colsurfb.2021.111641
Received 7 October 2020; Received in revised form 28 December 2020; Accepted 13 February 2021
Available online 18 February 2021

robust gel [26]. However, it is difficult to form stable elastic gels of PFOB that can be used in clinical settings. Adding specific polymer amphiphiles into perfluorocarbons could effectively assist to form a long-term stable emulsion gel. Previous research has demonstrated the benefits and enhancement provided by the addition of amphiphilic block copolymers [8,21,27]. However, to the best of our knowledge, the systematic structural and rheological studies of water-in-PFC nanoemulsions with various concentrations of amphiphilic copolymers have not been conducted.

In the present work, we investigated the effects of adding the triblock copolymers Pluronic® F127 (F127) into PFOB-based water-in-PFC nanoemulsion solutions on the related phase behaviors and rheological properties, which resulted in long-term stable nanoemulsion gels with tunable elasticity. F127 is an amphiphilic poly(ethylene oxide)-poly(propylene oxide)-poly(ethylene oxide) (PEO-PPO-PEO) triblock copolymer, widely used in pharmaceutical formulations. We expect that the hydrophilic (PEO) endblocks of copolymers will enter the water phase and assist in forming stable cores of the nanoemulsion droplets, while the relatively hydrophobic poly(propylene oxide) (PPO) chains will reside in the continuous fluorocarbon phase and may form loops on the droplet surface or bridges between droplets. The stability and microstructure of prepared series of emulsion gels with various compositions have been characterized by confocal microscopy, small-angle X-ray scattering (SAXS) and small-angle neutron scattering (SANS) for detailed examinations. Related rheological experiments have been performed to investigate the relationship between the structure and rheological properties. The temperature-dependent and thermoreversible behaviors was verified by investigating viscoelastic moduli. The scale of rheological properties could be tuned by adjusting the surfactant concentration and volume fraction of the aqueous phase. The biocompatibility of PFC materials and tunable mechanical properties of the obtained nanoemulsion gels make them a promising system for biomedical applications.

## 2. Materials and methods

### 2.1. Materials

Perfluorooctyl bromide ($CF_3(CF_2)_6CF_2Br$, abbreviated as PFOB), Pluronic® F127 ($PEO_{101}$-$PPO_{56}$-$PEO_{101}$, abbreviated as F127), and Zonyl® FSO-100 ($F(CF_2)_{7.5}(CH_2CH_2O)_8H$, abbreviated as FSO) were obtained from Sigma Aldrich. Deuterium oxide ($D_2O$, 99.8 atom% D) and fluorescein isothiocyanate (FITC) were obtained from Acros Organics. Nanopure water was used in all sample preparation, except SANS samples which were prepared with $D_2O$.

### 2.2. Sample preparation

Previously published phase diagrams of water, FSO, and perfluorocarbons suggest that a stable water-in-oil emulsion may be formed at room temperature with 1:1 ratios of water to PFC, and at FSO concentrations in the range of 10−22 wt% [28]. Unless otherwise noted, for all samples described herein, the concentration of FSO was kept constant at 15 wt%, with varying amounts of PFOB, water, and F127. Aqueous solutions of F127 were prepared by first dissolving prescribed amounts of F127 in water at concentrations from 0.5 to 12 wt%. The obtained dispersions were stirred for one day to ensure complete dissolution, and then equilibrated for one day to remove possible air bubbles. The F127 solutions were then mixed with PFOB and FSO, stirred for 5 h at room temperature, and then held still for another 5 h for equilibration. It was found that F127 did not dissolve directly in PFOB phase. This suggests that in our final samples, all F127 triblock copolymers are associated with nanoemulsion droplets in water phase rather than self-assembling into F127 micelles in the continuous PFOB phase.

We refer to samples using the following nomenclature: $\varphi = 0.58$, 4 wt % F127. The volume fraction of droplets, $\varphi$, which assumes ideal mixing, is calculated as the volume of the aqueous phase plus the volume of FSO over the total volume. This is consistent with how $\varphi$ is defined in other work on nanoemulsions with added block copolymers. The existence of water-in-oil nanoemulsion structure was verified by SANS, as described below. The stated concentration of triblock copolymer F127 (4 wt%) is the concentration of F127 relative to the aqueous phase instead of the overall concentration in the sample.

### 2.3. Rheology

A TA AR2000 stress-controlled rheometer was used to investigate the storage modulus, loss modulus, and viscosity. The linear viscoelastic region was determined by a stress sweep, and then the storage modulus $G'$ and loss modulus $G''$ are obtained by performing a frequency sweep. Viscosity was obtained by steady flow experiments at low shear rate. Temperature sweeps were used to investigate the thermal properties of the rheology from 10 °C to 35 °C.

### 2.4. Small-angle X-ray scattering (SAXS)

Samples were transferred into 0.1 mm thickness quartz capillary tubes and sealed using epoxy, then placed in a SAXS vacuum channel for testing. The SAXS experiments were conducted on a Molecular Metrology SAXS instrument at the W.M. Keck Nanostructures Laboratory at the University of Massachusetts Amherst. The instrument generates X-rays with a wavelength of $\lambda = 1.54$ Å and utilizes a 2-D multiwire detector with a sample-to-detector distance of 1.5 m. For transparent samples, SAXS data were collected for 50 min. For opaque samples, it took 4 h to obtain enough scattering contrast. The intensity was reduced and normalized by the Polar® software.

### 2.5. Confocal microscopy

A Leica DM-IRBE confocal optical microscopy was used to investigate sample homogeneity and possible phase separation at the microscale. Samples were prepared as above, with the hydrophilic dye FITC added to the aqueous phase at a concentration of 20 ppm prior to sample mixing.

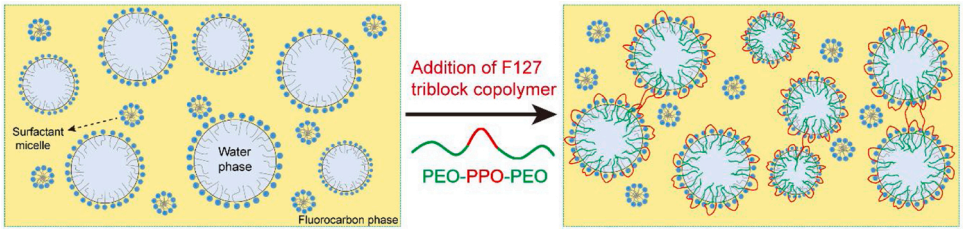


**Fig. 1.** Schematic diagram of the system of PFOB/water/FSO with F127 triblock copolymers. The copolymers form loops and bridges on nanoemulsion droplets with PFOB as continuous phase and water as droplet core. Not drawn to scale.

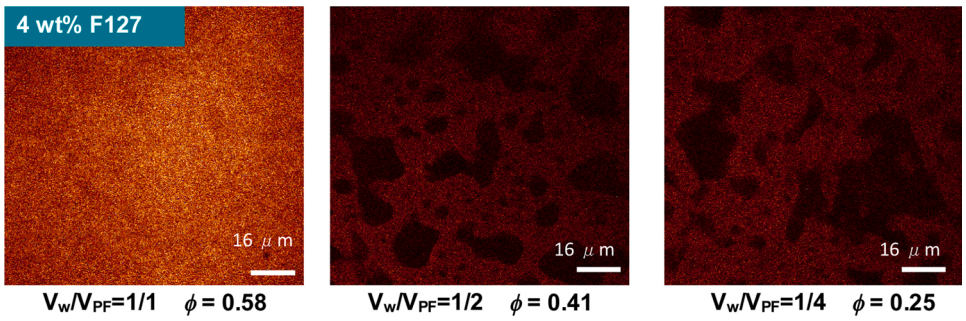


**Fig. 2.** Representative confocal micrographs of samples of $\varphi$ = 0.25-0.58, 4 wt% F127, $T$ = 25 °C. Samples at lower $\varphi$ show evidence of phase separation.

### 2.6. Small-angle neutron scattering (SANS)

Scattering experiments were conducted at the NG-3 beamline with a wavelength of 6 Å at the National Center for Neutron Research (NCNR), National Institute for Standards and Technology (NIST) (Gaithersburg, MD). Samples for SANS were prepared as above, except that $H_2O$ was replaced by $D_2O$. Samples were loaded into 1-mm thick quartz cells. Some samples were centrifuged to remove air bubbles before loading the cells to the slots of SANS facility. The distances from samples to the detector were 4 m and 13.18 m for high $q$ and low $q$ regime, and the spectra were collected for 5 min and 3 min, respectively. The combined $q$ range is from 0.001 $Å^{-1}$ to 0.2 $Å^{-1}$. Spectra were obtained at 25 °C for investigation of composition effects and from 10 °C to 32 °C for exploration of temperature effects. There are 5 min of equilibrium for each temperature. Data reduction and normalization were performed using standard techniques and all SANS data reported in this work are on an absolute scale.

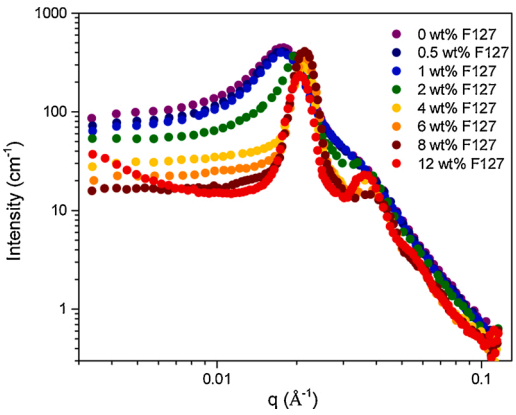


**Fig. 3.** SANS spectra for samples with $\varphi$ = 0.58, 0 – 12 wt% F127, $T$ = 25 °C.

## 3. Results and discussion

### 3.1. Formation and stability of nanoemulsions

Based on previously published phase diagrams, the PFOB/water/FSO system shows a formation of water-in-oil nanoemulsion only for $T >$ 40 °C [28]. It is expected that the addition of amphiphilic copolymers could promote the formation of self-assembled emulsions gel system (Fig. 1). Considering the potential for these systems to be used in biomedical applications, it is desirable to have stable systems at temperatures ranging from ambient temperature to physiological conditions (i.e., 25– 35 °C). Thus, it is necessary to firstly verify the temperature and concentration space over which stable solutions were formed with designed compositions of our systems.

Samples with 15 wt% FSO, volume fraction $\varphi$ = 0.58, and various concentrations of F127 from 0 to 12 wt% were prepared and evaluated. It was observed that all samples with varied concentrations of copolymer formed stable and transparent systems at ambient temperature. The translucent and unchanged outlooks of these samples suggested the existence of nanoemulsions inside samples, which was also verified with SANS in the following part. As shown in Fig. S1, samples containing 0–1 wt% F127 appeared to be in liquid state as emulsions while samples became elastic gels above 2 wt% concentrations of triblock copolymer. Detailed investigations were performed in the subsequent rheological experiments. The gelling of samples with higher F127 concentration could be explained by the enhanced association brought by the fluorinated surfactant and the added amphiphilic copolymer, which resulted in the formation of associative gels.

Confocal microscopy was also applied to confirm if any phase separation exists in these samples on the microscale. Fig. 2 shows micrographs of samples at 4 wt% F127 with varying volume fractions dyed by hydrophilic FITC. No phase separation was observed for samples at $\varphi$ = 0.58, indicating the nanoemulsion system with such $\varphi$ reached phase equilibrium [29,30]. However, samples at lower $\varphi$ displayed evidence of phase separation for the 4 wt% F127 system, which implies the threshold of minimum volume fraction of aqueous phase required in the stable water-in-fluorocarbon system.

Additionally, samples with different surfactant concentrations were investigated for potential effects on the system. Results showed that samples with higher and lower FSO concentrations were found to be opaque at room temperature (Fig. S2) while samples at intermediate concentration (15 wt%) became clear and transparent at 25 °C. Although detailed structural studies of opaque phases in certain samples were not performed, previous work of Schubert and Kaler suggests that the opaque phases may correspond to a lamellar liquid crystal, which may not be beneficial to the potential applications [28]. Considering the emphasis of this work is on exploring the stable systems with droplet nanostructures, the majority of SANS, SAXS, and rheology studies reported below focus on samples with an FSO concentration of 15 wt% and $\varphi$ = 0.58.

### 3.2. Microstructure: SANS and SAXS studies

In order to compare the internal structure of all samples, SANS and SAXS were used to evaluate the differences in nano-scale structures. SANS spectra on systems with $\varphi$ = 0.58 and varying amounts of F127 are shown in Fig. 3, which includes sample range from the neat nanoemulsion (0 wt% F127) to 12 wt% F127. All spectra displayed the characteristic scattering from spherical objects [31], suggesting the possible formation of emulsion droplets in the sample. Moreover, it was observed that the increased amount of F127 from 0 wt% to 12 wt% resulted in the sharpening of the primary peak and the appearance of higher-order peaks, which indicates some ordering of droplets were formed at higher F127 concentrations inside the systems. The SANS spectra do not have sufficient resolution to determine the nature of the ordering in systems at higher F127 concentrations. However, SAXS

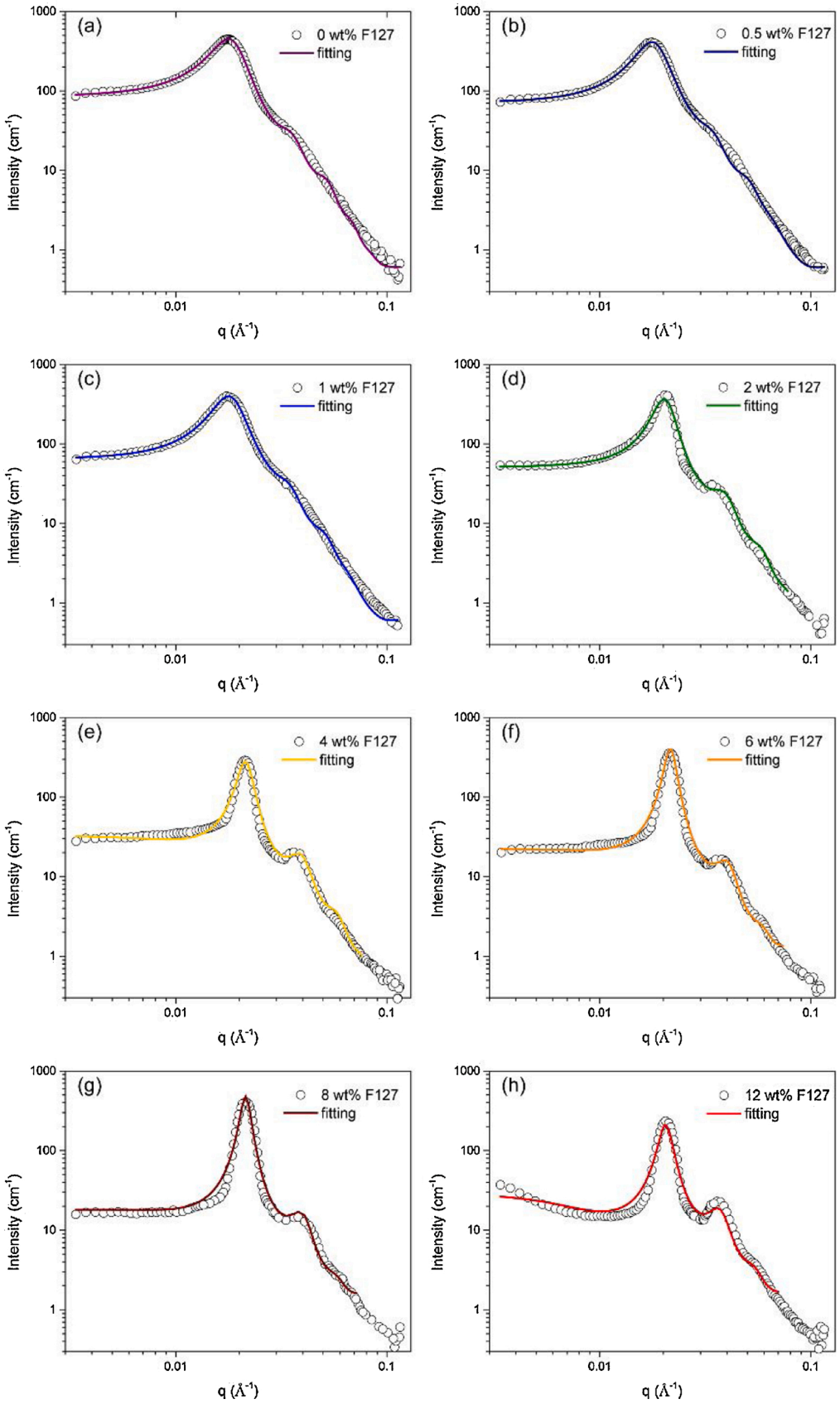


**Fig. 4.** SANS spectra and fittings of samples with $\varphi = 0.58$, 0-12 wt% F127, $T = 25$ °C. Spectra for samples with 2 wt% and 4 wt% F127 were manually fit.

profile confirms that the formed droplets show some short-range ordering in nanoscale corresponding to a hexagonal close-packed structure [32]. In Fig. S3, representative profile of sample with 4 wt% F127 displays the characteristic size of droplets as a *d*-spacing of ~30 nm, where the *d*-spacing is obtained as $d = 2\pi/q_{max}$.

In order to interpret the SANS data quantitively, SANS spectra were fit using established data-fitting routines [33]. The scattered intensity can be expressed as:

$$I = N(\Delta\rho)^2 P(q) S(q) \quad (1)$$

where *P(q)* is the form factor, *S(q)* is the structure factor, and *N* is the number density of the scatters. As mentioned above, the spectra are characteristic of spherical scatters. Thus, we choose to use a spherical core-shell form factor for all samples:

$$P(q) = \frac{\text{scale}}{V_s^3}\left[\frac{3V_c(\rho_c-\rho_s)j_1(qr_c)}{qr_c} + \frac{3V_s(\rho_s-\rho_{solv})j_1(qr_s)}{qr_s}\right]^2 + \text{bkg} \quad (2)$$

where $V_s$ is the volume of the whole particle, $V_c$ is the volume of the core, $r_c$ is the radius of the core, *t* is the thickness of the shell, $r_s$ is the radius of the particle, $\rho_c$ is the scattering length density (SLD) of the core, $\rho_s$ is the SLD of the shell, $\rho_{solv}$ is the SLD of the solvent, $j_1(x) = (\sin x - x\cos x)/x^2$, $r_s = r_c + t$, $V_s = (4\pi/3)r_s^3$, and $V_c = (4\pi/3)r_c^3$. Polydispersity in the core size was accounted for by averaging over a Schulz distribution of radii [34].

The structure factor *S(q)* contains the information about spatial arrangement of the particles relative to an arbitrary origin. For an isotropic solution, the orientational average can be calculated as:

$$S(q) = 1 + 4\pi n_p \int_0^\infty [g(r) - 1]\frac{\sin qr}{qr} r^2 dr \quad (3)$$

where *g(r)* can be calculated from Ornstein-Zernicke (O-Z) equation:

$$h(r) = g(r) - 1 = c(r) + n\int c(|\vec{r} - \vec{x}|)h(x)d\vec{x} \quad (4)$$

An additional closure relation between *c(r)* and *h(r)* is needed to solve the O-Z equation. We attempted to fit our data using three different models: a hard sphere potential with the Percus-Yevick (P-Y) closure, a square-well potential with the mean spherical approximation, and a perturbation solution of the P-Y closure with a sticky hard sphere potential. The most physically reasonable values for the parameters, which we judged based on both goodness-of-fit and low relative errors in the fit parameters of < 10%, were obtained with the square-well potential:

$$u(r) = \begin{cases} \infty & r \le \sigma \\ -U_0 & \sigma < r < \lambda\sigma \\ 0 & r > \lambda\sigma \end{cases} \quad (5)$$

where $\lambda$ is the width of square well defined in multiples of the particle diameter ($\sigma$), $U_0$ is the square well depth, and *r* is the distance from the center of a sphere [35]. However, there are some limitations to this approach. For example, it is known that use of the square-well potential with the mean spherical approximation yields the best agreement with Monte Carlo simulations of square-well fluids for $U_0 < 1.5\ kT$ and $\varphi < 0.08$. Considering that our samples are at considerably higher volume fractions, the obtained well depths are significantly higher than 1.5 *kT* for nearly all samples as well as the volume fractions are much greater than 0.08 but still smaller than 0.74. Nevertheless, as this model was the only one that yielded physically reasonable results, we have used the results of data-fitting with this model to interpret our results. Additionally, parameters for samples with 2 wt% and 4 wt% were fit manually due to issues with convergence of the fitting software for these samples; this resulted in no calculated errors for the fitting parameters for these samples.

Due to the equal ratio of water to PFOB in our samples, it is necessary to verify that we have water-in-fluorocarbon droplets, rather than fluorocarbon-in-water droplets. We attempted to fit our data assuming both scenarios. Only when considering the water-in-fluorocarbon emulsion did we obtain physically reasonable values for fitting parameters. Assuming fluorocarbon-in-water emulsion often led to negative values for the core radius and/or the shell thickness, which makes no sense for physical emulsion droplets. Thus, fittings of our scattering data confirm that we prepared nanoemulsions comprising water-in-fluorocarbon droplets.

**Table 1**
Structural parameters of emulsion droplets from spherical core-shell model. Spectra for samples with 2 wt% and 4 wt% F127 were manually fit and no fitting errors were obtained. Length ($r_s$) is defined as the sum of radius of core ($r_c$) and thickness (*t*).

| % F127 | Radius (Å) | Thickness (Å) | Length (Å) | Volfraction | Well depth (kT) |
|---|---|---|---|---|---|
| 0 | 119.0 ± 0.4 | 63.0 ± 0.6 | 182.0 ± 1.0 | 0.271 ± 0.002 | 2.8 ± 0.4 |
| 0.5 | 115.2 ± 0.4 | 63.7 ± 0.4 | 178.9 ± 0.8 | 0.258 ± 0.001 | 1.1 ± 0.1 |
| 1 | 112.8 ± 0.5 | 64.9 ± 0.4 | 177.7 ± 0.9 | 0.260 ± 0.002 | 1.1 ± 0.1 |
| 2 | 100.0 | 65.0 | 165.0 | 0.400 | 20.0 |
| 4 | 93.0 | 68.0 | 161.0 | 0.490 | 30.0 |
| 6 | 71.2 ± 0.6 | 91.3 ± 0.7 | 162.5 ± 1.3 | 0.439 ± 0.002 | 1597.1 ± 42.9 |
| 8 | 76.8 ± 1.2 | 84.7 ± 1.2 | 161.5 ± 2.4 | 0.469 ± 0.002 | 836.4 ± 18.8 |
| 12 | 79.9 ± 1.1 | 83.8 ± 0.9 | 163.7 ± 2.0 | 0.495 ± 0.001 | 1413 ± 50.9 |

Fittings of all scattering profiles and corresponding parameters obtained from the polydisperse spherical core-shell model are shown in Fig. 4 and Table 1. For most samples, the droplet radius plus shell thickness is roughly half of the *d*-spacing obtained from SAXS. This is physically reasonable since the *d*-spacing characterized by SAXS refers to the distance between two scattering centers of droplets, which is the approximate length scale of the nanoemulsion structure. The shell thickness increased with increasing concentration of F127, reaching a maximum at 6 wt% of F127 and then decreasing at higher concentration of F127. The radius showed a reverse trend, exhibiting a minimum value at 6 wt% F127. This suggests that the PEO blocks of F127 assist in forming smaller water droplet cores, leading to decreasing radius. Meanwhile, the PPO midblocks in the continuous PFC phase tended to stretch out and may act as bridges between droplets at higher F127 concentrations, resulted in the increasing value of thickness of droplets [36].

The trend of square well potential $U_0$, or strength of attraction is not clear at low triblock copolymer concentration but increases to reach a peak, and then decreases with higher concentration. Although the values for $U_0$ are quite high and may not be quantitatively accurate due to limitations of the square-well model, it is clear that addition of triblock polymers induces stronger attractions between droplets. Interestingly, the maximum attraction between droplets occurs at 6 wt% F127. Although we must be careful not to over-interpret these data, this behavior is directly mirrored in the elastic modulus, as described further below. Close examination of the SANS spectra at 12 wt% F127 shows an upturn at low *q* that cannot be captured accurately by the fitting model. This may indicate some type of phase separation on the microscale such as the formation of small domains that are richer in both droplets and F127 chains. It is known that similar types of samples display a phase separation that is equivalent to a gas-liquid transition in small molecule systems [30,37,38]. It is not clear what effect the formation of such a phase would have on the inter-droplet attraction and rheology, but it may act to decrease the effective droplet volume fraction and F127 concentration in the majority phase.

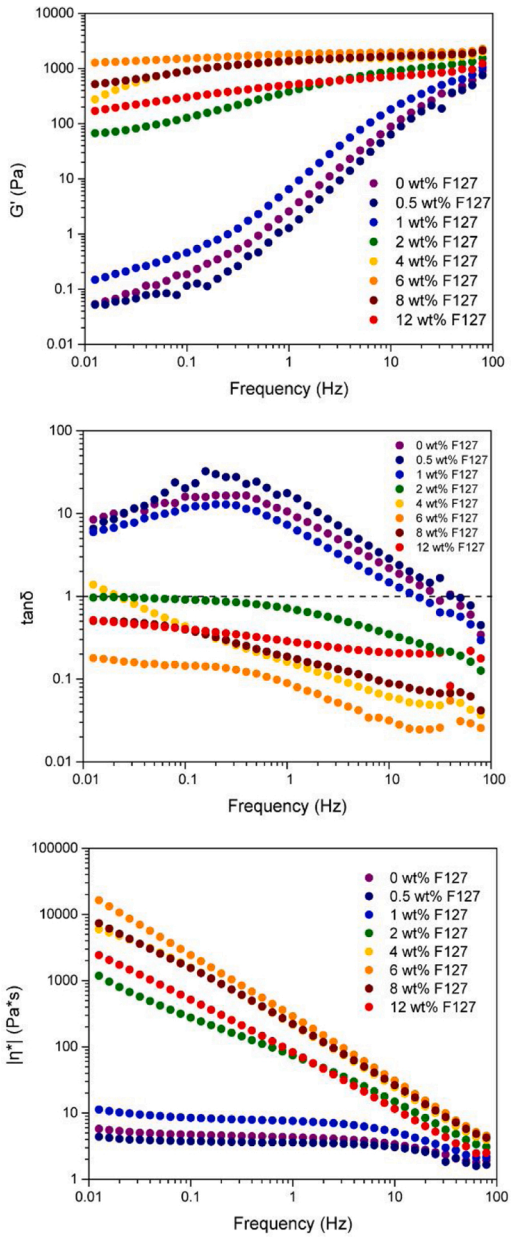


**Fig. 5.** Elastic modulus, tanδ and complex viscosity of samples at $\varphi = 0.58$, 0-12 wt% F127, $T = 20$ °C.

### 3.3. Rheology and analysis of structure-rheology relationships

In order to explore the relationship between the structure and rheological properties of samples, oscillatory rheology experiments were carried out on samples with various concentration of F127 at 20 °C. The obtained parameters including $G'$, tan $\delta$, and $|\eta^*|$ are shown in Fig. 5. There is a non-monotonic dependence of both $G'$ and $|\eta^*|$ on F127 concentration, with the maximum value of these parameters occurring at 6 wt% F127. As discussed above, this may be due to some sort of micro-phase separation at high F127 concentrations and the highest elastic modulus verifies the rationality of obtained strength of attractions between droplets from fitting model even though results exceeded the limitation.

Based on the value of tan $\delta$ in Fig. 5, these samples underwent a transition from liquids to elastic gels as F127 concentration increased. This was also quantified through following experiments. Although pure F127 copolymer in aqueous solutions can form gels, the gel-liquid transition in our system occurs between 2–4 wt% F127. This is far below the gelation concentration as 16 wt% of F127 in its neat aqueous solution at 25 °C [39,40]. This reveals that the added triblock copolymer was involved in formation of the PFOB/water/FSO emulsion gel system which helped enhance the stability of droplets with only a small amount of added F127.

**Table 2**
Theoretical Parameters from Classical Rubber Elasticity Theory.

| %F127 | $n$ | $\nu$ ($10^{22}$/m$^3$) | $G_{0,\mathrm{th}}$ (Pa) | $G_{0,ex}$(Pa) | $f$ |
|---|---|---|---|---|---|
| 0 | 0 | 0 | 0 | 59.0 | NA |
| 0.5 | 2.08 | 8.66 | 356 | 54.9 | 0.154 |
| 1 | 4.07 | 17.3 | 712 | 53.0 | 0.074 |
| 2 | 6.52 | 34.6 | 1424 | 71.2 | 0.050 |
| 4 | 12.1 | 69.3 | 2848 | 231.9 | 0.081 |
| 6 | 18.5 | 104 | 4272 | 937.1 | 0.219 |
| 8 | 24.5 | 139 | 5696 | 593.7 | 0.104 |
| 12 | 38.2 | 208 | 8545 | 575.2 | 0.067 |

To connect the rheology and various parameters that characterize the structure and inter-droplet forces, the above obtained rheological data is used to determine any possible relationships between them. There are two common concepts in theoretical descriptions of associative polymers: the fraction of elastically effective chains and the fraction of bridging chains. The fraction of elastically effective chains, $f$, is the fraction of chains that are connected to the infinite network of chains in the system. Not all bridging chains are elastically effective due to the topology of the network. Theoretical descriptions of triblock copolymers attached to spherical surfaces suggest that the maximum attainable value for the fraction of bridging chains is 1/3 [41].

Based on this, we can estimate the fraction of elastically effective chains from our data using results from classical rubber elasticity theory and transient network theory [42–44]:

$$G_{0,\mathrm{th}} = \nu kT \tag{6}$$

$$f = G_{0,\mathrm{exp}} / G_{0,\mathrm{th}} \tag{7}$$

where $\nu$ is the number density of elastically effective chains, $G_{0,\mathrm{th}}$ is the theoretical modulus assuming that all chains are elastically effective, and $G_{0,\mathrm{exp}}$ is the experimentally-determined high frequency elastic modulus. The number density of elastically effective chains is expressed as:

$$\nu = num_{polymer} / V_{total} \tag{8}$$

where $V_{total}$ is the total volume of sample and $num_{polymer}$ is number of polymer chains. The average number of polymers on droplets, $n$, is calculated as following:

$$\mathrm{n} = \mathrm{num.}_{\mathrm{polymers}} / \mathrm{num.}_{\mathrm{droplet}} \tag{9}$$

where

$$num_{droplet} = V_{total}\phi \Big/ \left[\frac{4}{3}\pi(r_c + t)^3\right] \tag{10}$$

The obtained parameters from above calculations are shown in Table 2. The maximum value of $f$, occurring at 6 wt% F127, is 0.219, which is much larger than the values at other concentrations. This indicates that significant bridging occurs between droplets in the 6 wt% F127 sample; that is, there is physical crosslinking of droplets by the PPO midblocks of the copolymers. Such a high fraction of bridging effect may lead to the increase of shell thickness and volume fraction. This also agrees with the previous results that samples with 6 wt% F127 show the largest thickness values in model fitting and the highest storage modulus in rheological experiments among all the samples.

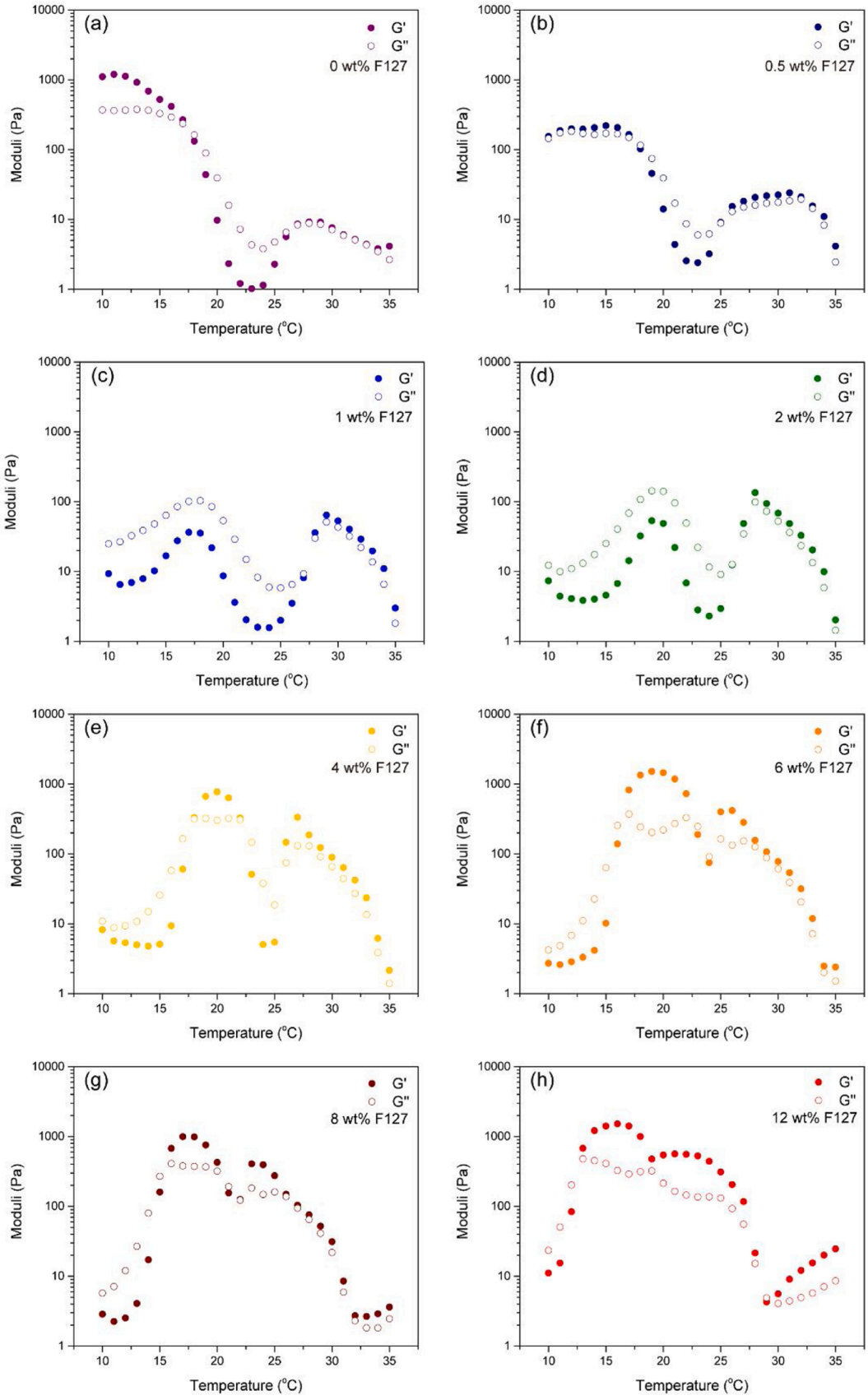


**Fig. 6.** Temperature sweeps (10-35 °C, equilibrium time 3 min for each °C, frequency 1 Hz) of the systems with $\varphi = 0.58$, 0-12 wt% F127.

### 3.4. Thermoreversible nature of gels

Temperature sweeps were performed in the range of $T = 10–35$ °C and these revealed the complexity of thermal effects on the emulsion gels. The emulsion system contains thermally-sensitive PEO and PPO chains from the triblock copolymer PEO-PPO-PEO and the surfactant FSO with the form $(CF_2)_n$-PEO. Thus, it is possible that complex influences will be imposed on these systems by changing the ambient temperature.

Fig. 6 shows the effects of temperature sweeps performed on systems with $\varphi = 0.58$ and 0–12 wt% F127 at a fixed frequency of 1 Hz. Samples below 4 wt% displayed the profile with $G'' > G'$ at room temperature and behaved as liquids, while these samples formed either elastic gels with $G' > G''$ or near-critical gels as $G' \sim G''$ at physiological temperature. This means the gelling process could be easily tuned by changing ambient temperature. Emulsion gels with such temperature-dependent behavior can find application as drug delivery vehicles and for use in cell encapsulation and tissue engineering. Samples with higher F127 concentration showed $G' > G''$ or $G' \sim G''$ at most temperatures tested, suggesting the amount of added triblock copolymer is crucial to the association and formation of emulsion gels.

For the purpose of exploring the potential practical application, the temperature cycling testing on elastic modulus and viscous modulus was performed. Fig. S4 revealed that viscoelastic moduli of 4 wt% sample acted as the functions of ambient temperature from 22 °C to 32 °C. Although there is a small degree of hysteresis, $G'$ and $G''$ are generally reversible through repeated heating and cooling cycles. Samples that have been repeatedly heated and cooled could recover their original rheological behavior. Thus, these systems with specific thermoresponsive and thermoreversible behavior are promising in potential applications. In addition, more discussion about the effects of volume fraction and surfactant concentration on the viscoelastic properties is available in the Supplemental Information.

## 4. Conclusions

In summary, the water-in-fluorocarbon emulsion gels were prepared and investigated with the addition of F127 triblock copolymer into the nanoemulsion system of PFOB/water/FSO. The stable compositions of water-in-fluorocarbon emulsion gels were obtained by tuning the amount of added fluorinated surfactant and the volume fraction of aqueous phase. The structures of transparent solution and gels were mainly investigated and were suggested to consist of water-in-oil nanoemulsion droplets. SAXS profiles suggests the existence of nanoscale ordering as hexagonal close-packed structure of droplets with a *d*-spacing of about 30 nm. SANS spectra with model fitting imply that as F127 concentration increases, the nanoemulsion gels undergo a structural change whereby water droplets decorated with copolymer in the fluorocarbon phase become smaller in size scale but increase in total numbers, and more physical crosslinking occurs caused by midblock bridging. The rheological properties were also tunable by changing compositions. A relatively low concentration of F127 triblock copolymer was applied to gel the nanoemulsion system. The maximum elastic modulus occurred in the 6 wt% F127 sample which agrees with the highest strength of attraction between droplets from the model fitting. The nanoemulsion gels are sensitive to temperature and switch from a liquid solution to gel state under physiological relevant temperatures, and the transition is reversible. Although we have focused on small-amplitude oscillatory measurements here, it is likely that the presence of the F127 also impacts the rheology in more complex ways, for example by modifying stress recovery behavior or other time-dependent phenomena, which should be explored in future studies.

## CRediT authorship contribution statement

**Jiachun Shen:** Formal analysis, Visualization, Writing - original draft. **Xiaoming Pan:** Investigation, Writing - original draft. **Surita R. Bhatia:** Conceptualization, Funding acquisition, Investigation, Project administration, Supervision, Writing - review & editing.

## Declaration of Competing Interest

The authors declare that they have no known competing financial interests or personal relationships that could have appeared to influence the work reported in this paper.

## Acknowledgments

Financial support for this work was provided by National Science Foundation awards CBET-1903189, CBET-0238873, and DGE-1922639. We acknowledge the support of the National Institute of Standards and Technology, U.S. Department of Commerce, in providing the neutron research facilities used in this work. The sponsors had no role in the study design; in the collection, analysis and interpretation of data; in the writing of the report; and in the decision to submit the article for publication.

## Appendix A. Supplementary data

Supplementary material related to this article can be found, in the online version, at doi:https://doi.org/10.1016/j.colsurfb.2021.111641.

## References

[1] M. Malmsten, Soft drug delivery systems, Soft Matter 2 (2006) 760–769.
[2] Z. Hami, M. Amini, M. Ghazi-Khansari, S.M. Rezayat, K. Gilani, Synthesis and in vitro evaluation of a pH-sensitive PLA–PEG–folate based polymeric micelle for controlled delivery of docetaxel, Colloids Surf. B Biointerfaces 116 (2014) 309–317.
[3] K. Shirk, C. Steiner, J.W. Kim, M. Marquez, C.J. Martinez, Assembly of colloidal silica crystals inside double emulsion drops, Langmuir 29 (2013) 11849–11857.
[4] Rk. Genç, G. Clergeaud, M. Ortiz, C.K. O'sullivan, Green synthesis of gold nanoparticles using glycerol-incorporated nanosized liposomes, Langmuir 27 (2011) 10894–10900.
[5] Q. Zhang, L. Li, Y. Li, L. Cao, C. Yang, Surface wetting-driven separation of surfactant-stabilized water–oil emulsions, Langmuir 34 (2018) 5505–5516.
[6] B.P. Binks, C.P. Whitby, Nanoparticle silica-stabilised oil-in-water emulsions: improving emulsion stability, Colloids Surf. A 253 (2005) 105–115.
[7] B. Ashrafi, M.H. Tootoonchi, R. Bardsley, R.D. Molano, P. Ruiz, E.A. Pretto Jr., C. A. Fraker, Stable perfluorocarbon emulsions for the delivery of halogenated ether anesthetics, Colloids Surf. B Biointerfaces 172 (2018) 797–805.
[8] R.A. Day, D.A. Estabrook, C. Wu, J.O. Chapman, A.J. Togle, E.M. Sletten, Systematic study of perfluorocarbon nanoemulsions stabilized by polymer amphiphiles, ACS Appl. Mater. Interfaces 12 (2020) 38887–38898.
[9] K. Hörmann, A. Zimmer, Drug delivery and drug targeting with parenteral lipid nanoemulsions—a review, J. Control Release 223 (2016) 85–98.
[10] M.P. Krafft, J.G. Riess, Perfluorocarbons: life sciences and biomedical uses dedicated to the memory of professor guy Ourisson, a true RENAISSANCE man, J. Polym. Sci. Part A 45 (2007) 1185–1198.
[11] E. Kissa, Fluorinated Surfactants and Repellents, CRC Press, 2001.
[12] D.M. Lemal, Perspective on fluorocarbon chemistry, J. Organ. Chem. 69 (2004) 1–11.
[13] M.R. Gherase, J.C. Wallace, A.R. Cross, G.E. Santyr, Two-compartment radial diffusive exchange analysis of the NMR lineshape of Xe 129 dissolved in a perfluorooctyl bromide emulsion, J. Chem. Phys. 125 (2006), 044906.
[14] E. Pisani, N. Tsapis, B. Galaz, M. Santin, R. Berti, N. Taulier, E. Kurtisovski, O. Lucidarme, M. Ourevitch, B.T. Doan, Perfluorooctyl bromide polymeric capsules as dual contrast agents for ultrasonography and magnetic resonance imaging, Adv. Funct. Mater. 18 (2008) 2963–2971.
[15] R. Díaz-López, N. Tsapis, M. Santin, S.L. Bridal, V. Nicolas, D. Jaillard, D. Libong, P. Chaminade, V. Marsaud, C. Vauthier, The performance of PEGylated nanocapsules of perfluorooctyl bromide as an ultrasound contrast agent, Biomaterials 31 (2010) 1723–1731.
[16] K. Chin, S.F. Khattak, S.R. Bhatia, S.C. Roberts, Hydrogel-perfluorocarbon composite scaffold promotes oxygen transport to immobilized cells, Biotechnol. Prog. 24 (2008) 358–366.
[17] S.F. Khattak, Ks. Chin, S.R. Bhatia, S.C. Roberts, Enhancing oxygen tension and cellular function in alginate cell encapsulation devices through the use of perfluorocarbons, Biotechnol. Bioeng. 96 (2007) 156–166.
[18] M.Q. Huang, Q. Ye, D.S. Williams, C. Ho, MRI of lungs using partial liquid ventilation with water-in-perfluorocarbon emulsions, Magn. Reson. Med. 48 (2002) 487–492.

[19] Y. Yao, M. Zhang, T. Liu, J. Zhou, Y. Gao, Z. Wen, J. Guan, J. Zhu, Z. Lin, D. He, Perfluorocarbon-encapsulated PLGA-PEG emulsions as enhancement agents for highly efficient reoxygenation to cell and organism, ACS Appl. Mater. Interfaces 7 (2015) 18369–18378.
[20] D. Spahn, Blood substitutes Artificial oxygen carriers: perfluorocarbon emulsions, Crit. Care 3 (1999) 1–5.
[21] C. Holtze, A. Rowat, J. Agresti, J. Hutchison, F. Angile, C. Schmitz, S. Köster, H. Duan, K. Humphry, R. Scanga, Biocompatible surfactants for water-in-fluorocarbon emulsions, Lab Chip 8 (2008) 1632–1639.
[22] K. Debbabi, F. Guittard, J. Eastoe, S. Rogers, S. Geribaldi, Reverse water-in-fluorocarbon microemulsions stabilized by new polyhydroxylated nonionic fluorinated surfactants, Langmuir 25 (2009) 8919–8926.
[23] S. Rocca, M. Stébé, Mixed concentrated water/oil emulsions (fluorinated/hydrogenated): formulation, properties, and structural studies, J. Phys. Chem. B 104 (2000) 10490–10497.
[24] X. Fu, S. Ohta, M. Kamihira, Y. Sakai, T. Ito, Size-controlled preparation of microsized perfluorocarbon emulsions as oxygen carriers via the shirasu porous glass membrane emulsification technique, Langmuir 35 (2019) 4094–4100.
[25] C.A. Fraker, A.J. Mendez, L. Inverardi, C. Ricordi, C.L. Stabler, Optimization of perfluoro nano-scale emulsions: the importance of particle size for enhanced oxygen transfer in biomedical applications, Colloids Surf. B Biointerfaces 98 (2012) 26–35.
[26] J. Ravey, M. Stébé, S. Sauvage, Water in fluorocarbon gel emulsions: structures and rheology, Colloids Surf. A 91 (1994) 237–257.
[27] C. Washington, S. King, Effect of electrolytes and temperature on the structure of a poly (ethylene oxide)− poly (propylene oxide)− poly (ethylene oxide) block copolymer adsorbed to a perfluorocarbon emulsion, Langmuir 13 (1997) 4545–4550.
[28] K.-V. Schubert, E. Kaler, Microemulsifying fluorinated oils with mixtures of fluorinated and hydrogenated surfactants, Colloids Surf. A 84 (1994) 97–106.
[29] B. Zheng, B. Zheng, A.J. Carr, X. Yu, D.J. McClements, S.R. Bhatia, Emulsions stabilized by inorganic nanoclays and surfactants: stability, viscosity, and implications for applications, Inorg. Chim. Acta Rev. (2020), 119566.
[30] T.D. Gamot, A.R. Bhattacharyya, T. Sridhar, F. Beach, R.F. Tabor, M. Majumder, Synthesis and stability of water-in-oil emulsion using partially reduced graphene oxide as a tailored surfactant, Langmuir 33 (2017) 10311–10321.
[31] N. Gorski, J. Kalus, Temperature dependence of the sizes of tetradecyltrimethylammonium bromide micelles in aqueous solutions, Langmuir 17 (2001) 4211–4215.
[32] C. Doe, H.-S. Jang, S.R. Kline, S.-M. Choi, Subdomain structures of lamellar and reverse hexagonal pluronic ternary systems investigated by small angle neutron scattering, Macromolecules 42 (2009) 2645–2650.
[33] S.K. Agrawal, N. Sanabria-DeLong, G.N. Tew, S.R. Bhatia, Structural characterization of PLA− PEO− PLA solutions and hydrogels: crystalline vs amorphous PLA domains, Macromolecules 41 (2008) 1774–1784.
[34] A. Guinier, G. Fournet, K.L. Yudowitch, Small-Angle Scattering of X-rays, 1955.
[35] R. Sharma, K. Sharma, The structure factor and the transport properties of dense fluids having molecules with square well potential, a possible generalization, Physica A 89 (1977) 213–218.
[36] T.J. Barnes, C.A. Prestidge, PEO− PPO− PEO block copolymers at the emulsion droplet− water interface, Langmuir 16 (2000) 4116–4121.
[37] G. Fleischer, F. Stieber, U. Hofmeier, H.-F. Eicke, On the dynamics of equilibrium networks: POE-b-PI-b-POE copolymers in H2O/AOT/Isooctane water in oil microemulsions, Langmuir 10 (1994) 1780–1785.
[38] C. Quellet, H.F. Eicke, G. Xu, Y. Hauger, Transient networks in ABA block copolymer-microemulsion systems, Macromolecules 23 (1990) 3347–3352.
[39] P.K. Sharma, M.J. Reilly, S.K. Bhatia, N. Sakhitab, J.D. Archambault, S.R. Bhatia, Effect of pharmaceuticals on thermoreversible gelation of PEO–PPO–PEO copolymers, Colloids Surf. B Biointerfaces 63 (2008) 229–235.
[40] P.K. Sharma, S.R. Bhatia, Effect of anti-inflammatories on Pluronic® F127: micellar assembly, gelation and partitioning, Int. J. Pharm. 278 (2004) 361–377.
[41] S.R. Bhatia, W.B. Russel, End-capped associative polymer chains between nanospheres: attractions in ideal solutions, Macromolecules 33 (2000) 5713–5720.
[42] K. Inomata, D. Nakanishi, A. Banno, E. Nakanishi, Y. Abe, R. Kurihara, K. Fujimoto, T. Nose, Association and physical gelation of ABA triblock copolymer in selective solvent, Polymer 44 (2003) 5303–5310.
[43] F. Tanaka, S. Edwards, Viscoelastic properties of physically crosslinked networks. 1. Transient network theory, Macromolecules 25 (1992) 1516–1523.
[44] M.S. Green, A.V. Tobolsky, A new approach to the theory of relaxing polymeric media, J. Chem. Phys. 14 (1946) 80–92.